VHL-P138R and VHL-L163R novel variants: mechanisms of VHL pathogenicity involving HIF-dependent and HIF-independent actions

Cecilia Mathó[1, 2], Celia Fernández[1], Jenner Bonanata[3], Xian-De Liu[4], Ayelén Martin[1], Ana Vieites[1], Gabriela Sansó[1], Marta Barontini[1], Eric Jonasch[4], Elena Laura Coitiño[3], Patricia A. Pennisi[1*]

[1]Centro de Investigaciones Endocrinológicas 'Dr. César Bergadá' (CEDIE)-CONICET,FEI, Hospital de Niños R. Gutiérrez, Div. Endocrinología, Argentina, [2]Departamento de Genética, Facultad de Medicina, Universidad de la República, Uruguay, [3]Laboratorio de Química Teórica y Computacional, Instituto de Química Biológica, Facultad de Ciencias, Universidad de la República, Uruguay, [4]University of Texas MD Anderson Cancer Center, United States

Submitted to Journal:
Frontiers in Endocrinology

Specialty Section:
Cancer Endocrinology

Article type:
Original Research Article

Manuscript ID:
854365

Received on:
13 Jan 2022

Revised on:
14 Feb 2022

Journal website link:
www.frontiersin.org

Conflict of interest statement

The authors declare that the research was conducted in the absence of any commercial or financial relationships that could be construed as a potential conflict of interest

Author contribution statement

PP conceived, designed, and directed the experimental research; CM, XL and EJ designed experiments; CM and MCF planned and carried out the experiments; AM collected data; AV, GS and MB performed genetic and clinical characterization of VHL patients; ELC designed and directed the computational component of this work and JB carried out all the molecular dynamics simulations; CM and MCF took the lead on writing the manuscript, under the supervision of PP and ELC (who wrote the in silico sections). All authors provided critical feedback and helped shape the research, analysis, and manuscript.

Keywords

VHL, von Hippel-Lindau, Novel variants, P138R, L163R, functional characterization, molecular dynamics

Abstract

Word count: 203

von Hippel-Lindau disease is an autosomal dominant cancer syndrome caused by mutations in the VHL tumor suppressor gene. VHL protein (pVHL) forms a complex (VBC) with Elongins B-C, Cullin2 and Rbx1. Although other functions have been discovered, the most described function of pVHL is to recognize and target hypoxia inducible factor (HIF) for degradation.
This work comprises the functional characterization of two novel variants of the VHL gene (P138R and L163R) that have been described in our center in patients with VHL disease by in vitro, in vivo and in silico approaches.
In vitro, we found that these variants have a significantly shorter half-life compared to wild type VHL, but still form a functional VBC complex. Altered fibronectin deposition was evidenced for both variants using immunofluorescence. In vivo studies revealed that both variants failed to suppress tumor growth. By means of molecular dynamics simulations, we inspected in silico the nature of the changes introduced by each variant in the VBC complex.
We have demonstrated the pathogenicity of P138R and L163R novel variants, involving HIF dependent and HIF independent mechanisms. These results provide the basis for future studies regarding the impact of structural alterations on post translational modifications that drive pVHL's fate and functions.

Contribution to the field

von Hippel-Lindau disease is an autosomal dominant cancer syndrome caused by mutations in the VHL tumor suppressor gene, which is among the ones recommended for return secondary findings in clinical sequencing. This work comprises the functional characterization of two novel variants of the VHL gene (P138R and L163R) that have been described in our center in patients with VHL disease by in vitro, in vivo and in silico approaches. VHL protein (pVHL) forms a complex -VBC- with Elongins B-C, Cullin2 and Rbx1. Our in vitro analyses tested the expression, half-lives, and functionality of the VBC complexes formed by the variants, as well as fibronectin expression and deposition. Our in vivo experiments showed that the variants failed to repress tumor growth. In silico studies of the VBC complex in hypoxic and normoxic conditions revealed slight changes compared to the wild-type protein. By these three different approaches we have demonstrated the pathogenicity of P138R and L163R novel variants, involving HIF dependent and HIF independent mechanisms. These results provide the basis for future studies regarding the impact of structural alterations on post translational modifications that drive pVHL's fate and functions, that can explain pathogenesis and could lead to targeted therapies for specific mutations.

Funding statement

Ministerio de Salud de la Nación, Instituto Nacional del Cáncer
Consejo Nacional de Investigaciones Científicas y Técnicas
No funds recieved for Open Acces publication fees

Ethics statements

Studies involving animal subjects
Generated Statement: The animal study was reviewed and approved by Comité de Etica, Hospital de Niños Dr. R. Gutiérrez. Buenos Aires, Argentina.

Studies involving human subjects
Generated Statement: No human studies are presented in this manuscript.

Inclusion of identifiable human data
Generated Statement: No potentially identifiable human images or data is presented in this study.

Data availability statement

Generated Statement: The raw data supporting the conclusions of this article will be made available by the authors, without undue reservation.

VHL-P138R and VHL-L163R novel variants: mechanisms of VHL pathogenicity involving HIF-dependent and HIF-independent actions

Cecilia Mathó[1#], María Celia Fernández[1], Jenner Bonanata[2], Xian-De Liu[3], Ayelen Martin[1], Ana Vieites[1], Gabriela Sansó[1], Marta Barontini[1], Eric Jonasch[3], E. Laura Coitiño[2], Patricia Alejandra Pennisi[1]*

[1] Centro de Investigaciones Endocrinológicas Dr. César Bergadá, CEDIE, CONICET-FEI-División de Endocrinología, Hospital de Niños Dr. Ricardo Gutiérrez, Gallo 1330, Ciudad Autónoma de Buenos Aires, C1425EFD, Argentina

[2] Laboratorio de Química Teórica y Computacional (LQTC), Instituto de Química Biológica, Facultad de Ciencias and Centro de Investigaciones Biomédicas (CEINBIO), Universidad de la República, Iguá 4225, Montevideo, 11400, Uruguay

[3] University of Texas M.D. Anderson Cancer Center, 1515 Holcombe Blvd, Houston, Texas, TX 77030, USA

***Correspondence:**
Patricia Pennisi
ppennisi@cedie.org.ar

***Correspondence on the computational contributions to this article:**
Prof. E. Laura Coitiño
laurac@fcien.edu.uy

[#]**Current address:** Departamento de Genética, Facultad de Medicina, Universidad de la República, Avenida General Flores 2125, Montevideo, CP 11800, Uruguay. ceciliamatho@fmed.edu.uy, mathocecilia@gmail.com

Keywords: VHL, von Hippel-Lindau, novel variants, P138R, L163R, functional characterization, molecular dynamics

Word count:4817

Number of figures: 6

Number of tables:2

ABSTRACT

von Hippel-Lindau disease is an autosomal dominant cancer syndrome caused by mutations in the *VHL* tumor suppressor gene. VHL protein (pVHL) forms a complex (VBC) with Elongins B-C, Cullin2 and Rbx1. Although other functions have been discovered, the most described function of pVHL is to recognize and target hypoxia inducible factor (HIF) for degradation.

This work comprises the functional characterization of two novel variants of the VHL gene (P138R and L163R) that have been described in our center in patients with VHL disease by *in vitro*, *in vivo* and *in silico* approaches.

In vitro, we found that these variants have a significantly shorter half-life compared to wild type VHL, but still form a functional VBC complex. Altered fibronectin deposition was evidenced for both variants using immunofluorescence. *In vivo* studies revealed that both variants failed to suppress tumor growth. By means of molecular dynamics simulations, we inspected *in silico* the nature of the changes introduced by each variant in the VBC complex.

We have demonstrated the pathogenicity of P138R and L163R novel variants, involving HIF dependent and HIF independent mechanisms. These results provide the basis for future studies regarding the impact of structural alterations on post translational modifications that drive pVHL's fate and functions.

1 INTRODUCTION

von Hippel–Lindau (VHL) disease is a hereditary autosomal dominant syndrome (1,2) which predisposes to the formation of cysts, and benign and malignant tumors in different organs(3). Clinically, VHL disease can be divided into two subtypes based on the absence (type 1) or presence (type 2) of pheochromocytoma (4).

VHL disease's incidence ranges from 1/36000 to 1/45000 live births(3,5), and is caused by mutations in the VHL tumor suppressor gene, which is located in the short arm of chromosome 3 (3p25-26)(3). Its coding sequence spans three exons and encodes a 213-amino-acidprotein (pVHL) widely expressed in human tissues(4,6).

The correct folding of pVHL is coupled to the formation of the VBC complex with Elongin B and Elongin C (7,8) The VBC complex together with Cullin 2 are part of the substrate-binding subunit of an E3 ubiquitin ligase that negatively regulates expression of the hypoxia-inducible transcription factors (HIFs) (9,10). At normal oxygen level, HIF-α is hydroxylated at proline residues, in this form is recognized by VHL, leading to rapid ubiquitination and degradation by the proteasome(11,12).In hypoxic conditions, the prolyl-hydroxylases are inactive and HIF-α is stabilized, dimerizes with HIF-β (constitutively expressed) and translocate to the nucleus (12,13). The dimer functions as a transcription factor, negatively regulating the expression of diverse hypoxia-inducible genes involved in metabolism, angiogenesis, and apoptosis(12,14). In the past years research has demonstrated that the SUMOylation of pVHL by the protein RSUME prevents the formation of the VBC complex, thus HIF-α is not degraded even under normal oxygen conditions(15,16). On the other hand, pVHL has HIF independent actions, such as microtubule stabilization(17), primary cilium formation(18) and extracellular matrix fibronectin assembly(19,20)which are also important for tumor development.

To this day, more than 500 VHL mutations have been reported according to the Human Gene Mutation Database (HGMD ®Professional 2020.3, accessed on November 5th , 2020). Interestingly,

most of the families presenting with pheochromocytoma (type 2 VHL disease) harbor missense mutations, while families with type 1 VHL disease usually present with gene deletions or nonsense mutations (21–24)In the present work we performed the functional characterization of two genetic variants (P138R and L163R) that have been described at our center in patients with VHL disease(25). P138R variant was identified in 5 patients of a family with Type 2B VHL. L163R variant was identified in 2 patients of a family with pheochromocytoma only (Type 2C VHL). The P138R variant implies the change of a proline for an arginine in the β domain of pVHL, involved the interaction with HIF α while the L163R (25)variant is located in the α domain, involved in the union with Elongins B and C. Through *in vitro, in vivo* and *in silico* studies we demonstrated the pathogenicity of P138R and L136R variants affecting not only pVHL capacity to form HIF's recognition complex and its functioning in pseudo hypoxic conditions but also some of HIF's independent actions.

2 MATERIALS AND METHODS

2.1 Site directed mutagenesis

The vector VHL-wt-Venus-Retro(26) and the Quikchange II XL Site-Directed Mutagenesis Kit were used following manufacturer´s protocols to perform the specific mutations P138R (CCA→CGA) and L163R (CTC→CGC). Mutations were verified by DNA sequencing in ABI PRISM 310 Genetic Analyzer (Applied Biosystems, Foster City, CA, USA).

2.2 Stable cell line development

HEK293T cells were used as a helper cell line in order to obtain retrovirus with the desired vectors as previously described by Dr. Ding (27). Briefly, HEK293T cells were transfected with 3 different vectors: 1) pcGp, 2) pVSVG and 3) either one of the following: GFP-Retro/ VHL-wt-Venus-Retro/ VHL-P138R-Venus-Retro/ VHL-L163R-Venus-Retro using Lipofectamine 3000 (Invitrogen, Carlsbad, CA, USA). Upon assembly, supernatant was used to infect RCC 786-0 cells (ATCC® CRL-1932™, American Type Culture Collection, Manassas, VA, USA) and after 20 hours selection was performed with 1 mg/ml of G418 antibiotic (Sigma Aldrich, St Luis, MO, USA). Four different cell lines were obtained expressing GFP, VHL-wt-Venus, VHL-P138R-Venus and VHL-L163R-Venus. All cell lines were cultured in high glucose Dulbecco's Modified Eagle's Medium (DMEM) supplemented with 10% FBS and maintained at 37 °C in a humidified 5% CO_2 environment.

2.3 Western blotting

Proteins were obtained as previously described (28) and resolved on a 12.5% SDS-PAGE. After transferred to PDVF membranes, blots were blocked and probed with different primary antibodies: VHL (BD Biosciences # 556347, diluted 1/5000), GFP (Santa Cruz sc-8334, diluted 1/1000), HIF 2α (Novus Biologicals NB100-122, diluted 1/1000), β actin(Cell Signaling #4970, diluted 1/1000), Elongin B (Santa Cruz sc-133090, diluted 1/500) and Elongin C (Santa Cruz sc-1559, diluted 1/500). The following secondary antibodies were used accordingly: anti rabbit (Cell Signaling #7074, diluted 1/5000), anti goat (Santa Cruz sc 2020, diluted 1/2000) and anti mouse (Cell Signaling #7076, diluted 1/2000).

2.4 Cell treatments

Cell lines were seeded on 6 well plates and incubated with either 50 µg/ml cycloheximide to interfere with protein synthesis, or 5µg/ml MG132 to inhibit the proteasome, or 100µM $CoCl_2$ (29) to simulate hypoxia. After treatment, proteins or RNA were extracted.

2.5 Immunoprecipitation

The amount of protein coming from GFP, WT VHL-Venus, P138R VHL-Venus and L163R VHL-Venus cell lines was determined by Bradford assay and 1mg of protein was immunoprecipitated using GFP-Trap®_A kit (Chromotek GmBH, Germany). The immunocomplexes were detected by western blot using the antibodies described above. Protein from WT VHL-Venus cell line was used as positive control and from the cell line expressing GFP as a negative one.

2.6 Real time PCR

Total RNA from the different cell lines was extracted with Direct-Zol RNA Kit (Zymo Research, Irvine, CA, USA) following manufacturer's protocol. To perform RT-qPCR, 1 µg of RNA from each sample was used together with random hexamers and Super Script II (Invitrogen, Carlsbad, CA). Resulting cDNA was diluted by 1:10, and 3 µl from each dilution was subject to qPCR in triplicates using Kapa Syber Fast qPCR master mix (Kapa Biosystems, Boston, MA) in Step One Plus Real-Time PCR System (Life Technologies, Carlsbad, CA). mRNA values were calculated using relative quantitation method and are presented as fold change compared to control conditions. Specific primers were designed to assess fibronectin, VEGFA and GLUT1 normalized to TATA box binding protein (TBP), or VHL and HIF-2α normalized to GAPDH (glyceraldehyde 3-phosphate dehydrogenase).

2.7 Fibronectin deposition by immunofluorescence

Using anti-fibronectin antibody combined with a secondary antibody conjugated with Cy5, matrix deposition by all cell lines was analyzed according to Debnath *et al* (30)protocol. Briefly, cells were plated on coverslips, fixed and permeabilized after 6 days of culture. Nuclei were dyed with Hoechst (5 µg/ml) and pictures taken on a Carl-Zeiss AxioScope A1 microscope.

2.8 Xenografts

Immunodeficient mice (N:NIH (S)- Fox 1^{nu}) were housed in standard conditions of 12 h light, 12 h dark cycle with water and food *ad libitum*, in accordance with National Institutes of Health guide for the care and use of laboratory animals(31).

A solution of 1 x 10^7 viable cells was injected subcutaneously on 6-8 weeks old male mice and monitored weekly for tumor development. At 16 weeks post cell injection or when tumor reached 2 cm diameter, mice were sacrificed, and tumor histology evaluated by Hematoxylin and Eosin (H&E) staining.

All animals were treated and cared for in accordance with standard international animal care protocols. All procedures were approved by the Animal Care and Use Committee of the Hospital de Niños Dr. Ricardo Gutiérrez.

2.9 Database search and online predictions

We searched for these variants in the Genome Aggregation Database (gnomAD)(32), dbSNP(33) and ClinVar (34) databases to look at allele frequency, and if they had been reported by other groups. We also used online tools that predict the effect of protein variants: SIFT(35),

Polyphen(36), Mutation Taster(37) and Human Splicing Finder(38). To classify these variants according to the American College of Medical Genetics Guidelines (39) we used VarSome(40).

2.10 *In silico* studies: Molecular dynamics simulations

The crystal structure of a human VBC:HIF-1α complex PDB 4AJY (X-Ray diffraction, 1.73 Å resolution) was used as starting structure (41). Missing residues of EloC (amino acids 106 to 118) were added using the SWISS-MODEL workspace (42,43). The following six macromolecular systems were considered: wild type and P138R and L163R variants of pVHL inserted in VBC:HIF-1α complexes, both under normoxia or hypoxia (the latter simulated replacing Hyp564 by Pro564 in HIF-1α). Lacking experimental structures of the two variants considered, *in silico* mutations were introduced by replacing the residue of interest at the native structure using the SWISS-PDB Viewer software (42). Protonation states of titratable residues were determined with PROPKA 3.0 (44), then all missing hydrogen atoms were added with the ProToss utility of the Proteins Plus server. All the systems were solvated with a truncated-octahedral box of TIP3P water 12 Å around the solute and neutralized with K^+ ions, using the *leap* module of AmberTools17 (45). Each of the systems was minimized (2000 steps applying a 500 kcal mol^{-1} $Å^{-2}$ harmonic potential over solute atoms, followed by 20000 steps without restraints), then heated to 310 K (500 ps molecular dynamics simulation, MD, in NVT ensemble) and equilibrated at 1 atm (1 ns MD simulation at 310 K in NPT ensemble), prior to run 400 ns of productive MD simulations (NPT, 310 K and 1 atm). Minimizations and MD simulations were carried out with the *pmemd.cuda* module of AMBER16 (45). Protein residues were treated using the AMBER *ff14SB* force field. An integration step of 2 fs was used, constraining bonds involving hydrogen with SHAKE algorithm (46). Temperature and pressure were controlled applying the Langevin thermostat (47) and the Monte Carlo barostat (48), respectively. An 8.0 Å cutoff was used for direct non-bonded interactions and the Particle Mesh Ewald (PME) method (49) applied to long-range electrostatic interactions. Trajectory processing and analysis was performed with *cpptraj* module of AmberTools 17. Trajectory convergence was monitored following Cα-RMSDs and flexibility examined by means of per-residue Cα-RMSF. Snapshots of the trajectory were clustered into 5 clusters —each one with a representative structure— using a hierarchical agglomerative algorithm. Binding free energies of HIF-1α to the VBC complex were calculated using the MM-PB(GB)SA methods (50). For those calculations, the first 50 ns of the trajectories were discarded, then 100 snapshots separated by 3.5 ns were used. Representative structures of clusters with appreciable population (> 10 %) were used to calculate the electrostatic potential of VBC using the APBS software (51) implemented in the APBS/PDB2PQR web server (52).

2.11 Statistical analysis

For Real Time PCR analysis, one-way ANOVA was used with a Tukey test post evaluation. The Chi square test was used to analyze the differences in tumor incidence and crosstab were created. Statistical significance was defined as a p-value of less than 0.05 and all data was graphed as mean ± standard deviation unless indicated otherwise.

3 RESULTS

3.1 P138R and L163R pVHL variants exhibit lower protein levels than WT pVHL

We analyzed the effect of P138R and L163R novel variants on VHL protein stability using Venus tagged proteins. Human 786–0 RCC cell line (VHL-deficient) was infected with retroviral vectors to stably express VHL-P138R-Venus, VHL-L163R-Venus and VHL-wt-Venus. Protein levels for both variants were significantly lower than those for VHL-wt-Venus (Fig. 1A). Assessed by RT-qPCR, mRNA levels showed that VHL-P138R-Venus and VHL-L163R-Venus variants were

similar and even higher than VHL-wt-Venus mRNA levels (Fig. 1B) suggesting that transcription levels are not responsible for the differences in protein levels evidenced by Western Blot.

Cell lines were treated with cycloheximide to inhibit protein translation and enable the determination of half-lives for both VHL variants and wt pVHL. After six hours, results showed that VHL-P138R-Venus, VHL-L163R-Venus have a significantly shorter half-life (≈1.2 hs and 1 hs, respectively) compared to VHL-wt-Venus' (≈3.4 hs) (Fig. 1C).

Inhibiting the proteasome with MG132 (proteasome inhibitor) significantly increased both variants' protein levels, achieving quantities comparable to wt VHL levels after MG132 treatment for case of P138R and slightly lower for L163R (Fig. 1D).

3.2 VBC complex formation is apparently diminished but still functional for P138R and L163R

To date, pVHL's most described function is its interaction and consequent downregulation of HIF-α protein subunits (53). To this end, pVHL needs to form the VBC complex (pVHL-Elongin B-Elongin C). Immunoprecipitation of GFP Trap showed a specific band of 25 kD for GFP alone and 50 kD on cells expressing GFP- pVHL-Venus Tag (Fig 2 A). Consistent with previous results (Figure 1A), pVHL levels are different for the wt and P138R and L163R variants resulting in less coimmunoprecipitation of Elongin B and C for the variants compared to wt VHL cell line (Fig 2 A). We calculated the ratio between the bands obtained: Elongin C/pVHL and Elongin B/pVHL for wt pVHL, P138R and L163R pVHL expressing cell lines. Ratios were normalized to wt pVHL's set as 1 and we observed that P138R immunoprecipitates less Elongin B and Elongin C (approximately 0.6) and L163R manages to immunoprecipitate a similar proportion of Elongin C but a lower quantity of Elongin B (0.25).

Since VBC complex was evidenced for both variants, we sought to evaluate its functionality. Firstly, the capacity of pVHL variants to downregulate HIF-2α was assessed. HIF-2α is overexpressed in the parental cell line used (786-0)(54) and its levels decrease significantly in the derived cell line expressing VHL-wt-Venus (Figure 2B lanes 1 and 2). Protein levels for both P138R and L163R cell lines (Figure 2B, lanes 3 and 4) were intermediate for HIF-2α assessed by Western blot although mRNA levels did not change in the different cell lines (Figure 2 B). To evidence the consequence of these intermediate levels of HIF-2α protein we quantified mRNA levels of two of its downstream targets: vascular endothelial growth factor (VEGF) and glucose transporter 1 (GLUT1) using qRT-PCR in normoxic and pseudohypoxic conditions (Figure 2 C). Despite different HIF-2α protein levels, mRNA levels in normoxia for VEGF and GLUT1 were similar amongst cell lines expressing wt, P138R and L163R pVHL (Figure 2C, upper panel). Under pseudohypoxic conditions we found significantly higher levels of VEGF and GLUT1 mRNAs on the variants cell lines compared to the one expressing wt pVHL (Figure 2 C, lower panel).

3.3 Altered fibronectin deposition in P138R pVHL and L163R pVHL with different RNA levels

pVHL is known to regulate fibronectin mRNA levels, although the underlying molecular mechanism hasn't been yet described. We assessed fibronectin mRNA levels in the 786-0 and 786-0 derived cell lines expressing VHL-wt-Venus, VHL-P138R-Venus and VHL-L163R-Venus by RT-qPCR. Cells expressing wt-VHL have higher fibronectin mRNA levels than the parental 786-0 which is pVHL null (Figure 3 A). Regarding the variants, P138R expression shows similar fibronectin mRNA levels to that of wt-VHL expressing cell line. On the other hand, L163R expression resulted in diminished fibronectin mRNA levels and significantly different to the wt-VHL, but comparable to the levels obtained for 786-0 cell line (Figure 3 A).

Fibronectin expression *per se* does not ensure its proper extracellular matrix organization. Using immunofluorescence we evidenced fibronectin deposition in the 786-0 cell line as a dotted pattern while in VHL-wt-Venus resulted in fibrillar network of fibronectin deposition (Figure 3 B). Both variants, P138R and L163R, failed to generate this fibrillar organization, demonstrating a pattern similar to that observed in the parental 786-0 cell line where pVHL is absent (Figure 3 B).

3.4 Cells expressing P138R and L163R pVHL do not suppress tumor growth as WT pVHL does

To test the tumor suppressor role of the novel variants, we injected the cell lines expressing wt-VHL, P138R and L163R pVHL into male nude mice. Also, 786-0 cell line was injected as an internal control for the experiments. In our hands, visible tumors were developed, on average, 9 weeks after injection for all the tested cell lines.

As expected, the ratio between the number of tumors developed and the number of sites injected was significantly higher in 786-0 compared to the cells expressing the wt-VHL protein. Moreover, P138R and L163R pVHL expressing cells developed more tumors when compared to wt-VHL cell line (Figure 4B). Contingency tables were obtained showing a significant difference between P138R, L163R or 786-0 cells with wt pVHL, where tumors developed in 55% (11/20 for both variants) or 40 % (4/10 for 786-0 cells) of the sites injected compared to a 10% for wt pVHL(3/30) (Figure 4B). Also, the variants showed a similar ratio of developed tumors to that of the parental cell line.

Hematoxylin and eosin staining confirmed that developed tumors had histological characteristics that are compatible with clear cell renal carcinoma (Figure 4C). These solid tumors were composed by atypical, polyhedral cells that have a large, acidophilic, or optically empty cytoplasm with large nuclei where its membrane was observed thickened and a prominent central nucleolus. Cells are grouped into clusters separated by thin collagen tracts through which small blood vessels pass (Figure 4C, I and II). Tumors had infiltrating growth towards neighboring tissues (Figure 4C, III) and showed histological signs of proliferative activity, evidenced by the numerous of mitotic figures found (Figure 4C, IV).

pVHL protein expression was verified on tumors developed by 786-0 cells, wt pVHL, P138R and L163R cell lines by Western blot. As shown in Figure 4D, pVHL was not detectable on 786-0 cells, and had higher levels on wt pVHL expressing cells compared to both variants (P138R and L163R).

3.5 Database search and online predictions

The results of our database and online prediction tools are summarized in Table 1.

Our variants were not found in the Genome Aggregation Database (gnomAD) which includes thousands of genomes and exomes, this information allows us to infer they have a very low allelic frequency. Most of the effect prediction tools used suggest both variants are deleterious. L163R was previously reported by our group and reported in ClinVar by a genetic testing laboratory that classifies it as a variant of unknown significance (VUS). Using VarSome to follow the ACMG guidelines for classification of new variants, they are classified as likely pathogenic (P138R) and Pathogenic (L163R).

3.6 *In silico* studies of VBC:HIF-1α complexes by MD simulations

Molecular dynamics simulations (MD) enabled us to inspect at a molecular level the effects of introducing P138R and L163R pVHL variants in the VBC:HIF complex structure and stability, flexibility of the protein components and other features relevant towards molecular recognition of pVHL by HIF (here represented by a 559-577 peptide fragment from HIF-1α containing either

hydroxyproline Hyp564 or P564 in a carboxyl-terminal oxygen-dependent CODD motif, as representative of normoxia and hypoxia, respectively) in the VBC complex as well as by other possible interactors.

All the six MD 400 ns simulations promptly converged, showing formation of structurally stable complexes in all the cases. Introducing variants P138R and L163R in pVHL appears not to considerably disrupt HIF-1α binding to VBC under normoxic conditions: as shown in Table 2, the three complexes display similar binding strength values. Although VBC:HIF-1α complexes still form as evidenced *in vitro* (Figure 2A), binding strength is significantly reduced in all the cases under hypoxia, particularly for variant P138R (see Table 2).

Global structural fluctuations in protein backbones appear to be smaller under hypoxia (when HIF-1**α** Hyp564 is replaced by P564) with respect to normoxia (See Figure S1 in the Supplementary Material). Differences in dynamic behavior among wild-type, P138R and L163R variants of pVHL are more pronounced under conditions representative of normoxia and accompanied by side-chain shifts in residues relevant for the pathophysiological functions of pVHL.

3.6.1 Structure and dynamics of VBC:HIF involving WT and P138R/L163R variants

No major changes are detected in the tertiary and secondary structure of the pVHL:HIF complexes after introduction of variants P138R and L163R. Introducing variants affects specific interactions at the level of amino acid side chains directly in their local environment and for L163R it is propagated far away into the pVHL:HIF-1α interface. P138R introduces changes in a loop comprised from residues 136 to 151.

3.6.2 Flexibility of the components of the multiproteic complex – RMSFs

pVHL backbone flexibility and VCB interunit adaptation in the VBC complex are essential features towards successfully recruiting Cullin 2 (Cul2) E3 ubiquitin ligase and HIF-1α (55). Under high oxygen conditions, P138R variant significantly increases pVHL backbone flexibility in the region around P138 substitution comprising residues 136 to 151 (Figure S1, left bottom). More precisely, while lining the floor of the β-domain in native pVHL, this region constitutes a hydrophobic patch from where P138 establishes direct hydrogen-bonding interactions with H115 -one of the well-known residues clamping HIF-1α Hyp564 at the B-interface of pVHL- and Y112. In the P138R variant, the more extended and charged Arg138 lays at the bottom of the β-domain but displaced outwards from the hydrophobic *core* and oriented towards helix H4 -On the opposite direction, both variants slightly reduce the flexibility of the protein in the region 86-96, also in the β-domain of pVHL, as a part of the HIF-1α binding surface (primary binding site S1, quite shallow, rigid (13,56)) including some of the well-conserved residues lining the Hyp564 binding cavity. No significant alterations are introduced by the L163R variant located in the α-domain of pVHL at the hydrophobic surface patch defining the interface with EloC where L163 establishes hydrophobic interactions with pVHL residues K159, L188 and a leucine from EloC. No significant alterations in flexibility are observed under conditions representative of hypoxia (Figure S1, panel C), other than a small reduction in the native protein around 86-96. Introducing variants in pVHL does not affect in a significant way HIF-1α flexibility (Figure S1, left bottom), which remains bound to VBC in all the cases with similar strengths under normoxia (Table 2). In the case of P138R, a small increase in flexibility is noticed under hypoxia in the region after Pro564 partially comprising the primary (S1) and secondary (S2) HIF binding sites to pVHL. Introduction of variants in pVHL also reduces EloB flexibility in the region comprising residues 77 to 90. Whereas L163R does not alter EloC flexibility respect to VBC formed with native pVHL, P138R induces a reduction, mainly in the region defined by residues 83 to 93.

3.7 Changes towards molecular interactions after introducing variants in pVHL

3.7.1 Electrostatic reorganization influencing molecular recognition properties

As shown in Figure 6, front view representations, HIF-1α binding site in the native VBC complex has two regions of clearly defined positive and negative electrostatic potential that may be guiding HIF-1α recognition and proper positioning. Introduction of both variants in pVHL induce charge redistribution reflected in the MEP and changes in the surface molecular shape, with an influence in molecular recognition.

3.7.2 Exposition to solvent (SASA) of relevant pVHL Lys residues: K159, K171 and K196

We calculated the solvent accessible surface area (SASA) for lysine residues 159, 171 and 196 which are targets for post-translational modifications. Figure S2 and Table S1 in the Supplementary Material show the results for each of these. K159 is the most buried of the three Lys identified as relevant in the interaction with NEDD8. L163R variant further reduces solvent exposure of K159 in several frames of simulation, and this residue is reoriented. K171 is the most exposed of the three Lys inspected and none of the variants affected its exposition. K196 is less exposed to solvent for the case of the L163R variant.

4 DISCUSSION

In this study we aimed to describe two novel variants of the von Hippel Lindau protein: P138R and L163R, which have been found in families with VHL disease and haven't been functionally characterized before.

Firstly, by western blot we observed lower protein levels of the variants when compared to wt pVHL and showed that they have significantly lower half-lives compared to wt pVHL. Other groups have reported similar results for other pVHL variants such as: S65W(57), N78S(57), Y98H (57,58), W117A (26), P138L (59), V155A (60), L158P (57), L158Q (60), Q164R (60), R167Q (57,61), R167W (58), L188Q (57), L188V (60). There are striking differences amongst other authors' results regarding the absolute value of wt pVHL and variants half-lives, even if we only consider those that use the same cycloheximide concentration (50µg/ml). To compare our results with previous studies, we calculated the ratio between wt pVHL and our variants' half-lives., resulting in 2.8 (P138R) and 3.4 (L163R), approximately. Lanikova *et al*(59) (have described P138L variant, obtaining different absolute values for the half-lives, but a similar ratio to the one reported here for P138R. If we compare mutations near L163R.: Park *et al* (58) have shown that Q164R's half-life was reduced ≈3 fold compared to wt, while V155A and L158Q≈5.5-6 fold. Ding *et al*(61) showed a ≈3 fold reduction of R167Q's half-life. When regarding absolute half-lives values, Bangiyeva *et al* (57) showed that after 2 hours of cycloheximide treatment, levels of L158P and R167Q diminished drastically, becoming very low or undetectable by western blot, resembling our results.

On the other hand, when cell lines were treated with the proteasome inhibitor MG132, we observed accumulation of wt pVHL, P138R and L163R. Both variants increased their levels in a higher proportion than wt pVHL. Taken together, the above data suggests that the lower protein levels observed for VHL-P138R-Venus and VHL-L163R-Venus are due to proteasomal degradation.

The most studied mechanism for pVHL proteasome-mediated degradation is UCP mediated polyubiquitination. Other authors have shown that UCP mediates the degradation of V155A, L158Q and Q164R variants(60). P138R and L163R variants do not involve the substitution of lysine residues (subject to ubiquitination) directly, but they could alter their surroundings, favoring their exposure and thus their ubiquitination. Particularly, for L163R variant, lysine 196 appears to be less exposed to the solvent, result that would not favor polyubiquitination of this residue. Given that the region of interaction of pVHL with UCP has not been determined yet, one could speculate that this region might vary its conformation as a result of changes introduced in the pVHL protein.

Therefore, an increase in the affinity of UCP for pVHL variants might explain their increased degradation compared to wt pVHL.

We showed that both pVHL variants maintain their ability to form a VBC complex, although it is apparently formed at a lower rate: P138R appears to bind less Elongin B and C , while L163R appears to bind Elongin C appropriately but less Elongin B. These results are in agreement with other groups' findings, since the majority of inherited *VHL* mutations are defective in Elongin B and C binding(62–65). Other groups have shown that variants close to P138R and L163R such as D121G (66), Q145H (67), F148A (61), V155A (60), Q164R (60) y R167Q(61,66,68) form less VBC Complex compared to wt pVHL, while L158P(69)and C162F(63,70) are unable to form this complex and therefore do not have the capacity to downregulate HIF-α subunits (69,71,72).

On the other hand, VBC complex formation itself does not ensure its functionality, as it must recognize HIF-α subunits in order to target them for proteasomal degradation. Ding *et al* (61) have shown that W117A and F148A mutations form less VBC complex and also lose their ability to interact with HIF-2α. We interrogated the capacity of the P138R and L163R pVHL variants to form a functional VBC complex and therefore accomplish the interaction and proteasome-mediated degradation of HIF-2α. By Western blot, intermediate levels of HIF-2α were observed by the cell lines expressing P138R and L163R, therefore we decided to evaluate the consequence of these intermediate levels by evaluating the expression (mRNA) of two target genes: VEGF and GLUT1. We showed that under normoxic conditions these genes exhibit the same regulation in cell lines expressing either the variants and wt pVHL. Nevertheless, after 24 hours of pseudohypoxia, significant, though subtle differences were observed between the cell lines expressing the variants compared to wt pVHL. As a consequence, variants' VBC complexes could not appropriately regulate HIF-2α levels under these experimental conditions. This result suggests that the novel pVHL variants might have a different behavior compared to wt pVHL under more physiologically challenging conditions. The results obtained *in silico* suggest that VBC-HIF-1α complexes formed by the variants are thermodynamically favorable because of their negative ΔG.

In summary, our results indicate that although the protein levels for P138R and L163R pVHL variants are lower compared to wt pVHL, these interact forming a functional VBC complex capable of targeting HIF-2α for proteasome mediated degradation.

As mentioned before, numerous pVHL HIF-independent mechanisms account for pVHL as a tumor suppressor (18,19,73). We decided to explore the relationship of these variants with fibronectin regulation since it has been explored since 1998 and is the most described HIF independent function to date(19). Other authors have shown that cell lines with pVHL mutants expression result in a defective fibronectin matrix deposition(19,71,74).

Our results indicate that although the novel variants exhibit a different regulation of fibronectin mRNA levels, they both fail in assembling a proper extracellular fibronectin matrix. For the L163R variant, less exposure to solvent of lysine 196 could explain a lower NEDDylation level and therefore the defective interaction with fibronectin, since NEDDylation has been described as a necessary switch for fibronectin interaction (75). These findings are speculative at this point and need to be tested *in vitro* in future studies.

The 786-0 cell line develops tumors when injected into nude mice, while clones of this cell line expressing wt-VHL do not, or in some cases they do but in a much smaller proportion of the injected mice, compared to 786-0. Our xenograft experiments revealed that P138R-pVHL and L163R-pVHL failed to suppress tumor growth, obtaining 11 tumors out of 20 sites injected with each variant (55% incidence), a similar proportion to the one obtained by parental 786-0 cell line which does not express pVHL (40% incidence). These results confirm the pathogenic role for P138R and L163R pVHL variants since they are unable to suppress tumor growth such as wt pVHL does. A study conducted by Ding *et al* (61) revealed that the amount of a missense mutated VHL

protein (R167Q) could impact its function suppressing tumorigenesis when proteasome is inhibited and this protein is therefore accumulated. Using the same approach and experimental tools, our pVHL variants were not able to compensate their functional deficiencies and demonstrated tumorigenic capacity suggesting that there are a variety of mechanisms driving tumor formation. Our work reinforces the importance of studying specific variants to identify their biological impact. This work sets the stage for mechanistic studies exploring the altered mechanisms that explain pathogenesis and could lead to more targeted therapies for specific mutations.

Overall, our results show that P138R and L163R pVHL variants can be classified as pathogenic since they failed to suppress tumor development in nude mice. Future studies are suggested for the elucidation of the mechanisms underlying their pathogenicity. In the current Omics era, our study sets the basis for future proteomics and genomics approaches to compare cell lines expressing these variants with the wt protein to fully understand this missense variants' global effects.

Captions for the figures

Figure 1: Reduction in protein levels and half-life for P138R and L163R pVHL variants. A) Representative western blot showing the levels of GFP and VHL protein obtained in each cell line and β-actin as loading control. B) Expression of VHL measured by qrPCR and graphed as fold change for P138R and L163R pVHL variants compared to pVHL WT. *p<0.0001, **p=0.424, One-way ANOVA and Tukey´s post-test. C) Proteins levels obtained by western blot after treatment with 50 µg/ml cycloheximide to inhibit protein translation. Quantification was done in order to plot the proportion of protein levels on the different time points evaluated. The dotted line indicates the 50%. D) Inhibition of proteasome by 5 µg/ml MG 132 for cell lines expressing WT, P138R and L163R pVHL variants. Results are shown by a representative western blot for VHL and β-actin. Relative quantification of the bands is shown under each line.

Figure 2: P138R and L163R pVHL variants form less VBC complexes without losing functionality. A) Representative western blot showing immunoprecipitation of GFP-trap for each cell line expressing GFP, VHL- WT, P138R or L163R. Membranes were blotted with anti-GFP, anti-VHL, anti-Elongin C and anti-Elongin B. B) Representative western blot showing the levels of HIF-2α protein and mRNA measured by RT-qPCR and graphed as fold change for 786-O, WT, P138R and L163R cell lines. C) VEGF and GLUT1 mRNA expression were calculated by RT-qPCR under normoxia or 24 hs of pseudohypoxia generated with 100 µM $CoCl_2$. Results are presented as fold change relative to pVHL WT expression. ns: not significant, * p<0.0001, **p=0.0401, ***p=0.0002 One-way ANOVA and Tukey´s post-test.

Figure 3: Differences in mRNA fibronectin expression for P138R and L163R pVHL variants with similar disrupted deposition pattern. A) Fibronectin mRNA expression of 786-O, WT, P138R and L163R cell lines. Results are presented as fold change compared to WT cells. Values are expressed as ± SD of three independent experiments performed in triplicates. ns: not significant, * p=0.0011, ** p=0.0030, *** p=0.0004, **** p=0.0042, ***p < 0.001, One-way ANOVA and Tukey´s post-test. B) Cell lines were cultured on coverslips to assess fibronectin deposition with anti-fibronectin Cy5 conjugated (in red) by immunofluorescence. Nuclei were dye with 5µg/ml Hoechst as shown in blue. Images were taken at 40X on a Carl-Zeiss AxioScope A1 microscope.

Figure 4: *In vivo* studies showed tumor development for P138R and L163R pVHL variants. A) Representative picture of nude mice and the tumors developed. The arrow points towards a tumor (upper panel). The bottom panel shows the macroscopical aspect of the tumors. B) Left plots represent the incidence obtained for each cell line when injected on immunodeficient mice and percentages are plot on the right panels. ns: not significant, *p=0.0306, **p=0.0005, Two-tails Chi square test. C) Histological features of the experimentally obtained tumors and stained with H&E.

Panel I, Tumor cells distributed as lobes of polyhedral cells separated by fine fibers of connective tissue (CT) and striated muscle (SM) 20x (Panel I). Panel II, a magnification of a sector of panel I, shows a connective septum with central endothelial nuclei corresponding to the capillary vessel (marked with black arrowheads), surrounded by tumor cells with nuclei (red arrows) with prominent central nucleolus; 100x. Panel III presented tumor infiltrating the neighboring striated muscle and the asterisks (*) indicate traces of tumor progression between the muscle bundles. Panel IV shows mitotic figures indicated with black arrows; 100x. D) Representative western blot showing the expression of VHL protein in the tumors developed by 786-O, WT, P138R and L163R cell lines. β-actin was blot as loading control.

Figure 5: 3D representative structures from MD simulations. A) VBC complex with pVHL:HIF-1α and pVHL:Elongin C interfaces where variants are located circled and evidencing relevant residues. B) and C) Overlapped representative structures for the most populated clusters from 400 ns MD simulation under normoxia. Circled residues correspond to pVHL variants amino acids P138R and L163R in B and C, respectively. Color code: green, wild type pVHL; yellow: P138R pVHL variant; red L163R pVHL variant.

Figure 6: *In silico* studies showed both reorganization in shape and/or surface electrostatic potential in pVHL variants. Molecular electrostatic potential (MEP) is mapped on the Connolly surface as calculated for WT and P138R or L163R pVHL variants. Representative structures were extracted from the most populated cluster from each MD simulation. Units of potential range from -7 to 7 kT/e (red negative, blue positive values). Relevant modifications in shape and/or surface MEP between WT and mutants are evidenced by placing black asterisks nearby. The interaction domains of pVHL with HIF and EloC/EloB are shown in the left for the each of the three views displayed.

Figures

Figure 1

Figure 2

Figure 3

Figure 4

Figure 5

Figure 6

Tables

Table 1-Databases and online predictions for our pVHL variants

Variant	ACMG Classification using VarSome	Databases			Mutation Effect Predictions			
		gnomAD (v3.1.2 &2.1.1)	dbSNP	ClinVar	SIFT	Polyphen	Mutation Taster	Human Splicing Finder
P138R	Likely Pathogenic	NA	NA	NA	Affect Protein Function	Probably damaging	Deleterious	New Donor Splice site
L163R	Pathogenic	NA	rs28940297	VUS	Affect Protein Function	Probably damaging	Deleterious	No significant impact on splicing signals

Table 2. MMPBGSA binding free-energies ($\Delta_b G$) for VBC:HIF-1α complexes

System	$\Delta_b G$ (MMPBSA, kcal mol^{-1})		
	Normoxia	Hypoxia	$\Delta(\Delta_b G)$
wild-type	−34 ± 12	−23 ± 12	**11**
P138R	−33 ± 08	−12 ± 10	**21**
L163R	−33 ± 09	−24 ± 10	**9**

5 Conflict of Interest

The authors declare that the research was conducted in the absence of any commercial or financial relationships that could be construed as a potential conflict of interest.

6 Author Contributions

PP conceived, designed, and directed the experimental research; CM, XL and EJ designed experiments; CM and MCF planned and carried out the experiments; AM collected data; AV, GS and MB performed genetic and clinical characterization of VHL patients; ELC designed and directed the computational component of this work and JB carried out all the molecular dynamics simulations; CM and MCF took the lead on writing the manuscript, under the supervision of PP and ELC (who wrote the *in silico* sections). All authors provided critical feedback and helped shape the research, analysis, and manuscript.

7 Funding

This work was supported by Instituto Nacional del Cáncer, Ministerio de Salud, Argentina (Grant 2014-2016, awarded to PP) and Consejo Nacional de Investigaciones Científicas y Técnicas, CONICET, Argentina (PIP#0100214, 2013-2015, awarded to PP).

8 Acknowledgments

AM and CM were recipients of Doctoral fellowships from CONICET. CM received a Bunge & Born fellowship. MCF is Assistant Researcher from CONICET. CM, JB and ELC are researchers of the Sistema Nacional de Investigadores (SNI, ANII-Uruguay) and PEDECIBA (MEC-UdelaR, Uruguay).

This paper is dedicated to the loving memory of Dr. Alicia Merlino (LQTC, UdelaR) who took part in early stages of this work, prematurely deceased on July 8th, 2018.

9 References

1. Friedrich CA. Von Hippel-Lindau syndrome. A pleomorphic condition. *Cancer* (1999) **86**:2478–2482.

2. Clark PE, Cookson MS. The von Hippel-Lindau gene: turning discovery into therapy. *Cancer* (2008) **113**:1768–1778.

3. Latif F, Tory K, Gnarra J, Yao M, Duh FM, Orcutt ML, Stackhouse T, Kuzmin I, Modi W, Geil L, et al. Identification of the von Hippel-Lindau disease tumor suppressor gene. *Science (80-)* (1993) **260**:1317–1320.

4. Kim WY, Kaelin WG. Role of VHL gene mutation in human cancer. *J Clin Oncol* (2004) **22**:4991–5004.

5. Cho HJ, Ki CS, Kim JW. Improved detection of germline mutations in Korean VHL patients by multiple ligation-dependent probe amplification analysis. *J Korean Med Sci* (2009) **24**:77–83.

6. GTEx Portal. Available at: https://gtexportal.org/home/gene/VHL#gene-transcript-browser-block [Accessed November 14, 2021]

7. McClellan AJ, Scott MD, Frydman J. Folding and quality control of the VHL tumor suppressor proceed through distinct chaperone pathways. *Cell* (2005) **121**:739–748. doi:10.1016/j.cell.2005.03.024

8. Melville MW, Mcclellan AJ, Meyer AS, Frydman J, Darveau A. The Hsp70 and TRiC / CCT

Chaperone Systems Cooperate In Vivo To Assemble the Von Hippel-Lindau Tumor Suppressor Complex The Hsp70 and TRiC / CCT Chaperone Systems Cooperate In Vivo To Assemble the Von Hippel-Lindau Tumor Suppressor Complex. (2003) **23**:3141–3151. doi:10.1128/MCB.23.9.3141

9. Pause A, Peterson B, Schaffar G, Stearman R, Klausner RD. Studying interactions of four proteins in the yeast two-hybrid system: structural resemblance of the pVHL/elongin BC/hCUL-2 complex with the ubiquitin ligase complex SKP1/cullin/F-box protein. *Proc Natl Acad Sci U S A* (1999) **96**:9533–9538. doi:10.1073/PNAS.96.17.9533

10. Pause A, Lee S, Worrell RA, Chen DY, Burgess WH, Linehan WM, Klausner RD. The von Hippel-Lindau tumor-suppressor gene product forms a stable complex with human CUL-2, a member of the Cdc53 family of proteins. *Proc Natl Acad Sci U S A* (1997) **94**:2156–2161. doi:10.1073/pnas.94.6.2156

11. Haase VH. The VHL/HIF oxygen-sensing pathway and its relevance to kidney disease. *Kidney Int* (2006) **69**:1302–1307.

12. Chan DA, Sutphin PD, Yen S-E, Giaccia AJ. Coordinate regulation of the oxygen-dependent degradation domains of hypoxia-inducible factor 1 alpha. *Mol Cell Biol* (2005) **25**:6415–6426. doi:10.1128/MCB.25.15.6415-6426.2005

13. Hon WC, Wilson MI, Harlos K, Claridge TD, Schofield CJ, Pugh CW, Maxwell PH, Ratcliffe PJ, Stuart DI, Jones EY. Structural basis for the recognition of hydroxyproline in HIF-1 alpha by pVHL. *Nature* (2002) **417**:975–978. doi:10.1038/nature00767nature00767 [pii]

14. Shen C, Kaelin Jr. WG. The VHL/HIF axis in clear cell renal carcinoma. *Semin Cancer Biol* (2013) **23**:18–25. doi:S1044-579X(12)00093-4 [pii]10.1016/j.semcancer.2012.06.001

15. Gerez J, Tedesco L, Bonfiglio JJ, Fuertes M, Barontini M, Silberstein S, Wu Y, Renner U, Páez-Pereda M, Holsboer F, et al. RSUME inhibits VHL and regulates its tumor suppressor

577 function. *Oncogene* (2015) **34**:4855–4866. doi:10.1038/onc.2014.407

578 16. Antico Arciuch VG, Tedesco L, Fuertes M, Arzt E. Role of RSUME in inflammation and
579 cancer. *FEBS Lett* (2015) **589**:3330–3335. doi:10.1016/j.febslet.2015.07.048

580 17. Hergovich A, Lisztwan J, Barry R, Ballschmieter P, Krek W. Regulation of microtubule
581 stability by the von Hippel-Lindau tumour suppressor protein pVHL. *Nat Cell Biol* (2003)
582 **5**:64–70. doi:10.1038/ncb899

583 18. Kuehn EW, Walz G, Benzing T. Von hippel-lindau: a tumor suppressor links microtubules
584 to ciliogenesis and cancer development. *Cancer Res* (2007) **67**:4537–4540.
585 doi:10.1158/0008-5472.CAN-07-0391

586 19. Ohh M, Yauch RL, Lonergan KM, Whaley JM, Stemmer-Rachamimov AO, Louis DN,
587 Gavin BJ, Kley N, Kaelin WG, Iliopoulos O. The von Hippel-Lindau Tumor Suppressor
588 Protein Is Required for Proper Assembly of an Extracellular Fibronectin Matrix. *Mol Cell*
589 (1998) **1**:959–968. doi:10.1016/S1097-2765(00)80096-9

590 20. Tang N, Mack F, Haase VH, Simon MC, Johnson RS. pVHL function is essential for
591 endothelial extracellular matrix deposition. *Mol Cell Biol* (2006) **26**:2519–2530.
592 doi:10.1128/MCB.26.7.2519-2530.2006

593 21. Stolle C, Glenn G, Zbar B, Humphrey JS, Choyke P, Walther M, Pack S, Hurley K, Andrey
594 C, Klausner R, et al. Improved detection of germline mutations in the von Hippel-Lindau
595 disease tumor suppressor gene. *Hum Mutat* (1998) **12**:417–423.

596 22. Kumar PS, Venkatesh K, Srikanth L, Sarma PVGK, Reddy AR, Subramanian S, Phaneendra
597 BV. Novel three missense mutations observed in Von Hippel-Lindau gene in a patient
598 reported with renal cell carcinoma. *Indian J Hum Genet* (2013) **19**:373–376.
599 doi:10.4103/0971-6866.120809

600 23. Maher ER, Webster AR, Richards FM, Green JS, Crossey PA, Payne SJ, Moore AT.

Phenotypic expression in von Hippel-Lindau disease: correlations with germline VHL gene mutations. *J Med Genet* (1996) **33**:328–332.

24. McNeill A, Rattenberry E, Barber R, Killick P, MacDonald F, Maher ER. Genotype-phenotype correlations in VHL exon deletions. *Am J Med Genet A* (2009) **149A**:2147–2151. doi:10.1002/ajmg.a.33023

25. Sansó G, Rudaz MCG, Levin G, Barontini M. Familial isolated pheochromocytoma presenting a new mutation in the von Hippel-Lindau gene. *Am J Hypertens* (2004) **17**:1107–1111. doi:10.1016/j.amjhyper.2004.06.013

26. Ding Z, German P, Bai S, Feng Z, Gao M, Si W, Sobieski MM, Stephan CC, Mills GB, Jonasch E. Agents that stabilize mutated von Hippel-Lindau (VHL) protein: results of a high-throughput screen to identify compounds that modulate VHL proteostasis. *J Biomol Screen* (2012) **17**:572–580. doi:10.1177/1087057112436557

27. Ding Z, Liang J, Lu Y, Yu Q, Songyang Z, Lin S-Y, Mills GB. A retrovirus-based protein complementation assay screen reveals functional AKT1-binding partners. *Proc Natl Acad Sci U S A* (2006) **103**:15014–15019. doi:10.1073/pnas.0606917103

28. Pennisi PA, Barr V, Nunez NP, Stannard B, Le Roith D. Reduced expression of insulin-like growth factor I receptors in MCF-7 breast cancer cells leads to a more metastatic phenotype. *Cancer Res* (2002) **62**:6529–6537.

29. Liu XD, Yao J, Tripathi DN, Ding Z, Xu Y, Sun M, Zhang J, Bai S, German P, Hoang A, et al. Autophagy mediates HIF2α degradation and suppresses renal tumorigenesis. *Oncogene* (2015) **34**:2450–2460. doi:10.1038/ONC.2014.199

30. Debnath J, Muthuswamy SK, Brugge JS. Morphogenesis and oncogenesis of MCF-10A mammary epithelial acini grown in three-dimensional basement membrane cultures. *Methods* (2003) **30**:256–268. doi:10.1016/S1046-2023(03)00032-X

31. Od Nih OO. *GUIDE LABORATORY ANIMALS for the CARE and USE of Eighth Edition*

Committee for the Update of the Guide for the Care and Use of Laboratory Animals. (2011).

32. Karczewski KJ, Francioli LC, Tiao G, Cummings BB, Alföldi J, Wang Q, Collins RL, Laricchia KM, Ganna A, Birnbaum DP, et al. The mutational constraint spectrum quantified from variation in 141,456 humans. *Nature* (2020) **581**:434–443. doi:10.1038/S41586-020-2308-7

33. Wheeler DL, Barrett T, Benson DA, Bryant SH, Canese K, Chetvernin V, Church DM, DiCuccio M, Edgar R, Federhen S, et al. Database resources of the National Center for Biotechnology Information. *Nucleic Acids Res* (2007) **35**:D5–D12. doi:10.1093/NAR/GKL1031

34. Landrum MJ, Lee JM, Benson M, Brown GR, Chao C, Chitipiralla S, Gu B, Hart J, Hoffman D, Jang W, et al. ClinVar: improving access to variant interpretations and supporting evidence. *Nucleic Acids Res* (2018) **46**:D1062–D1067. doi:10.1093/NAR/GKX1153

35. Sim NL, Kumar P, Hu J, Henikoff S, Schneider G, Ng PC. SIFT web server: predicting effects of amino acid substitutions on proteins. *Nucleic Acids Res* (2012) **40**:W452–W457. doi:10.1093/NAR/GKS539

36. Adzhubei IA, Schmidt S, Peshkin L, Ramensky VE, Gerasimova A, Bork P, Kondrashov AS, Sunyaev SR. A method and server for predicting damaging missense mutations. *Nat Methods* (2010) **7**:248–249. doi:10.1038/NMETH0410-248

37. Steinhaus R, Proft S, Schuelke M, Cooper DN, Schwarz JM, Seelow D. MutationTaster2021. *Nucleic Acids Res* (2021) **49**:W446–W451. doi:10.1093/NAR/GKAB266

38. Desmet FO, Hamroun D, Lalande M, Collod-Bëroud G, Claustres M, Béroud C. Human Splicing Finder: an online bioinformatics tool to predict splicing signals. *Nucleic Acids Res* (2009) **37**: doi:10.1093/NAR/GKP215

39. Richards S, Aziz N, Bale S, Bick D, Das S, Gastier-Foster J, Grody WW, Hegde M, Lyon

E, Spector E, et al. Standards and guidelines for the interpretation of sequence variants: a joint consensus recommendation of the American College of Medical Genetics and Genomics and the Association for Molecular Pathology. *Genet Med* (2015) **17**:405–423. doi:10.1038/gim.2015.30

40. Kopanos C, Tsiolkas V, Kouris A, Chapple CE, Albarca Aguilera M, Meyer R, Massouras A. VarSome: the human genomic variant search engine. *Bioinformatics* (2019) **35**:1978–1980. doi:10.1093/BIOINFORMATICS/BTY897

41. Van Molle I, Thomann A, Buckley DL, So EC, Lang S, Crews CM, Ciulli A. Dissecting fragment-based lead discovery at the von Hippel-Lindau protein:hypoxia inducible factor 1α protein-protein interface. *Chem Biol* (2012) **19**:1300–1312. doi:10.1016/J.CHEMBIOL.2012.08.015

42. Guex N, Peitsch MC. SWISS-MODEL and the Swiss-PdbViewer: an environment for comparative protein modeling. *Electrophoresis* (1997) **18**:2714–2723. doi:10.1002/ELPS.1150181505

43. Waterhouse A, Bertoni M, Bienert S, Studer G, Tauriello G, Gumienny R, Heer FT, De Beer TAP, Rempfer C, Bordoli L, et al. SWISS-MODEL: homology modelling of protein structures and complexes. *Nucleic Acids Res* (2018) **46**:W296–W303. doi:10.1093/NAR/GKY427

44. Olsson MHM, SØndergaard CR, Rostkowski M, Jensen JH. PROPKA3: Consistent Treatment of Internal and Surface Residues in Empirical pKa Predictions. *J Chem Theory Comput* (2011) **7**:525–537. doi:10.1021/CT100578Z

45. D. S. C. D.A. Case, T.E. Cheatham, III, T.A. Darden, R.E. Duke, T.J. Giese, H. Gohlke AWG, D.Greene, N. Homeyer, S. Izadi, A. Kovalenko, T.S. Lee, S. LeGrand, P. Li, C. Lin, J. Liu T, Luchko, R. Luo, D. Mermelstein, K.M. Merz, G. Monard, H. Nguyen, I. Omelyan, A. Onufriev F, Pan, R. Qi, D.R. Roe, A.Roitberg, C. Sagui, C.L. Simmerling, W.M. Botello-

675 Smith, J. Swails RC, Walker, J. Wang, R.M. Wolf, X.Wu, L. Xiao, D.M. York PAK.
676 AMBER 2017. San Francisco (2017).

677 46. J.-P. Ryckaert, G. Ciccotti HJCB. Numerical integration of the cartesian equations of motion
678 of a system with constraints: molecular dynamics of n-alkanes. *J Comput Phys* (1977)
679 **23**:327–341.

680 47. M. P. Allen DJT. *Computer simulation of liquids*. New York: Oxford University Press
681 (1991).

682 48. J. Åqvist, P. Wennerström, M. Nervall, S. Bjelic BOB. Molecular dynamics simulations of
683 water and biomolecules with a Monte Carlo constant pressure algorithm. *Chem Phys Lett*
684 (2004) **384**:288–294.

685 49. U. Essmann, L. Perera, M. L. Berkowitz, T. Darden, H. Lee LGP. A smooth particle mesh
686 Ewald method. *J Chem Phys* (1995) **103**:8577–8593.

687 50. Genheden S, Ryde U. The MM/PBSA and MM/GBSA methods to estimate ligand-binding
688 affinities. *Expert Opin Drug Discov* (2015) **10**:449–461.
689 doi:10.1517/17460441.2015.1032936

690 51. Baker NA, Sept D, Joseph S, Holst MJ, McCammon JA. Electrostatics of nanosystems:
691 application to microtubules and the ribosome. *Proc Natl Acad Sci U S A* (2001) **98**:10037–
692 10041. doi:10.1073/PNAS.181342398

693 52. Unni S, Huang Y, Hanson RM, Tobias M, Krishnan S, Li WW, Nielsen JE, Baker NA. Web
694 servers and services for electrostatics calculations with APBS and PDB2PQR. *J Comput*
695 *Chem* (2011) **32**:1488–1491. doi:10.1002/JCC.21720

696 53. Maher ER, Neumann HP, Richard S. von Hippel-Lindau disease: a clinical and scientific
697 review. *Eur J Hum Genet* (2011) **19**:617–23. doi:ejhg2010175 [pii]10.1038/ejhg.2010.175

54. Carroll VA, Ashcroft M. Role of hypoxia-inducible factor (HIF)-1alpha versus HIF-2alpha in the regulation of HIF target genes in response to hypoxia, insulin-like growth factor-I, or loss of von Hippel-Lindau function: implications for targeting the HIF pathway. *Cancer Res* (2006) **66**:6264–70. doi:10.1158/0008-5472.CAN-05-2519

55. Nguyen HC, Yang H, Fribourgh JL, Wolfe LS, Xiong Y. Insights into Cullin-RING E3 ubiquitin ligase recruitment: structure of the VHL-EloBC-Cul2 complex. *Structure* (2015) **23**:441–449. doi:10.1016/J.STR.2014.12.014

56. Min JH, Yang H, Ivan M, Gertler F, Kaelin WG, Pavietich NP. Structure of an HIF-1alpha -pVHL complex: hydroxyproline recognition in signaling. *Science* (2002) **296**:1886–1889. doi:10.1126/SCIENCE.1073440

57. Bangiyeva V, Rosenbloom A, Alexander AE, Isanova B, Popko T, Schoenfeld AR. Differences in regulation of tight junctions and cell morphology between VHL mutations from disease subtypes. *BMC Cancer* (2009) **9**:229.

58. Schoenfeld AR, Davidowitz EJ, Burk RD. Elongin BC complex prevents degradation of von Hippel-Lindau tumor suppressor gene products. *Proc Natl Acad Sci U S A* (2000) **97**:8507–8512. doi:10.1073/PNAS.97.15.8507

59. Lanikova L, Lorenzo F, Yang C, Vankayalapati H, Drachtman R, Divoky V, Prchal JT. Novel homozygous VHL mutation in exon 2 is associated with congenital polycythemia but not with cancer. *Blood* (2013) **121**:3918–3924. doi:10.1182/blood-2012-11-469296

60. Park KS, Kim JH, Shin HW, Chung KS, Im DS, Lim JH, Jung CR. E2-EPF UCP regulates stability and functions of missense mutant pVHL via ubiquitin mediated proteolysis. *BMC Cancer* (2015) **15**: doi:10.1186/S12885-015-1786-8

61. Ding Z, German P, Bai S, Reddy a S, Liu X-D, Sun M, Zhou L, Chen X, Zhao X, Wu C, et al. Genetic and pharmacological strategies to refunctionalize the von Hippel Lindau R167Q mutant protein. *Cancer Res* (2014) **74**:3127–3136. doi:10.1158/0008-5472.CAN-13-3213

723 62. Iliopoulos O, Kibel a, Gray S, Kaelin WG, Kaelin Jr. WG. Tumour suppression by the
724 human von Hippel-Lindau gene product. *Nat Med* (1995) **1**:822–826. doi:10.1038/nm0895-
725 822

726 63. Hansen WJ, Ohh M, Moslehi J, Kondo K, Kaelin WG, Welch WJ. Diverse effects of
727 mutations in exon II of the von Hippel-Lindau (VHL) tumor suppressor gene on the
728 interaction of pVHL with the cytosolic chaperonin and pVHL-dependent ubiquitin ligase
729 activity. *Mol Cell Biol* (2002) **22**:1947–1960. doi:10.1128/MCB.22.6.1947-1960.2002

730 64. Lonergan KM, Iliopoulos O, Ohh M, Kamura T, Conaway RC, Conaway JW, Kaelin WG.
731 Regulation of hypoxia-inducible mRNAs by the von Hippel-Lindau tumor suppressor
732 protein requires binding to complexes containing elongins B/C and Cul2. *Mol Cell Biol*
733 (1998) **18**:732–741. doi:10.1128/MCB.18.2.732

734 65. Kishida T, Lerman MI, Zbar B, Stackhouse TM, Chen F. Cellular proteins that bind the von
735 Hippel-Lindau disease gene product: mapping of binding domains and the effect of missense
736 mutations. *Cancer Res* (1995) **55**:4544–4548.

737 66. Hacker KE, Lee CM, Rathmell WK. VHL type 2B mutations retain VBC complex form and
738 function. *PLoS One* (2008) **3**: doi:10.1371/JOURNAL.PONE.0003801

739 67. Miller F, Kentsis A, Osman R, Pan ZQ. Inactivation of VHL by tumorigenic mutations that
740 disrupt dynamic coupling of the pVHL.hypoxia-inducible transcription factor-1alpha
741 complex. *J Biol Chem* (2005) **280**:7985–7996. doi:10.1074/JBC.M413160200

742 68. Rathmell WK, Hickey MM, Bezman NA, Chmielecki CA, Carraway NC, Simon MC. In
743 vitro and in vivo models analyzing von Hippel-Lindau disease-specific mutations. *Cancer*
744 *Res* (2004) **64**:8595–8603.

745 69. Clifford SC, Cockman ME, Smallwood AC, Mole DR, Woodward ER, Maxwell PH,
746 Ratcliffe PJ, Maher ER. Contrasting effects on HIF-1alpha regulation by disease-causing

pVHL mutations correlate with patterns of tumourigenesis in von Hippel-Lindau disease. *Hum Mol Genet* (2001) **10**:1029–1038. doi:10.1093/HMG/10.10.1029

70. Knauth K, Bex C, Jemth P, Buchberger A. Renal cell carcinoma risk in type 2 von Hippel-Lindau disease correlates with defects in pVHL stability and HIF-1alpha interactions. *Oncogene* (2006) **25**:370–377. doi:10.1038/SJ.ONC.1209062

71. Hoffman MA, Ohh M, Yang H, Klco JM, Ivan M, Kaelin Jr. WG, Kaelin WG. von Hippel-Lindau protein mutants linked to type 2C VHL disease preserve the ability to downregulate HIF. *Hum Mol Genet* (2001) **10**:1019–1027. doi:10.1093/HMG/10.10.1019

72. Wiesener MS, Seyfarth M, Warnecke C, Jürgensen JS, Rosenberger C, Morgan N V., Maher ER, Frei U, Eckardt KU. Paraneoplastic erythrocytosis associated with an inactivating point mutation of the von Hippel-Lindau gene in a renal cell carcinoma. *Blood* (2002) **99**:3562–3565. doi:10.1182/BLOOD.V99.10.3562

73. Li M, Kim WY. Two sides to every story: the HIF-dependent and HIF-independent functions of pVHL. *J Cell Mol Med* (2011) **15**:187–195. doi:10.1111/J.1582-4934.2010.01238.X

74. Stickle NH, Chung J, Klco JM, Hill RP, Kaelin WG, Ohh M. pVHL modification by NEDD8 is required for fibronectin matrix assembly and suppression of tumor development. *Mol Cell Biol* (2004) **24**:3251–3261. doi:10.1128/MCB.24.8.3251

75. Russell RC, Ohh M. NEDD8 acts as a "molecular switch" defining the functional selectivity of VHL. *EMBO Rep* (2008) **9**:486–491. doi:10.1038/EMBOR.2008.19

Figure 1.TIF

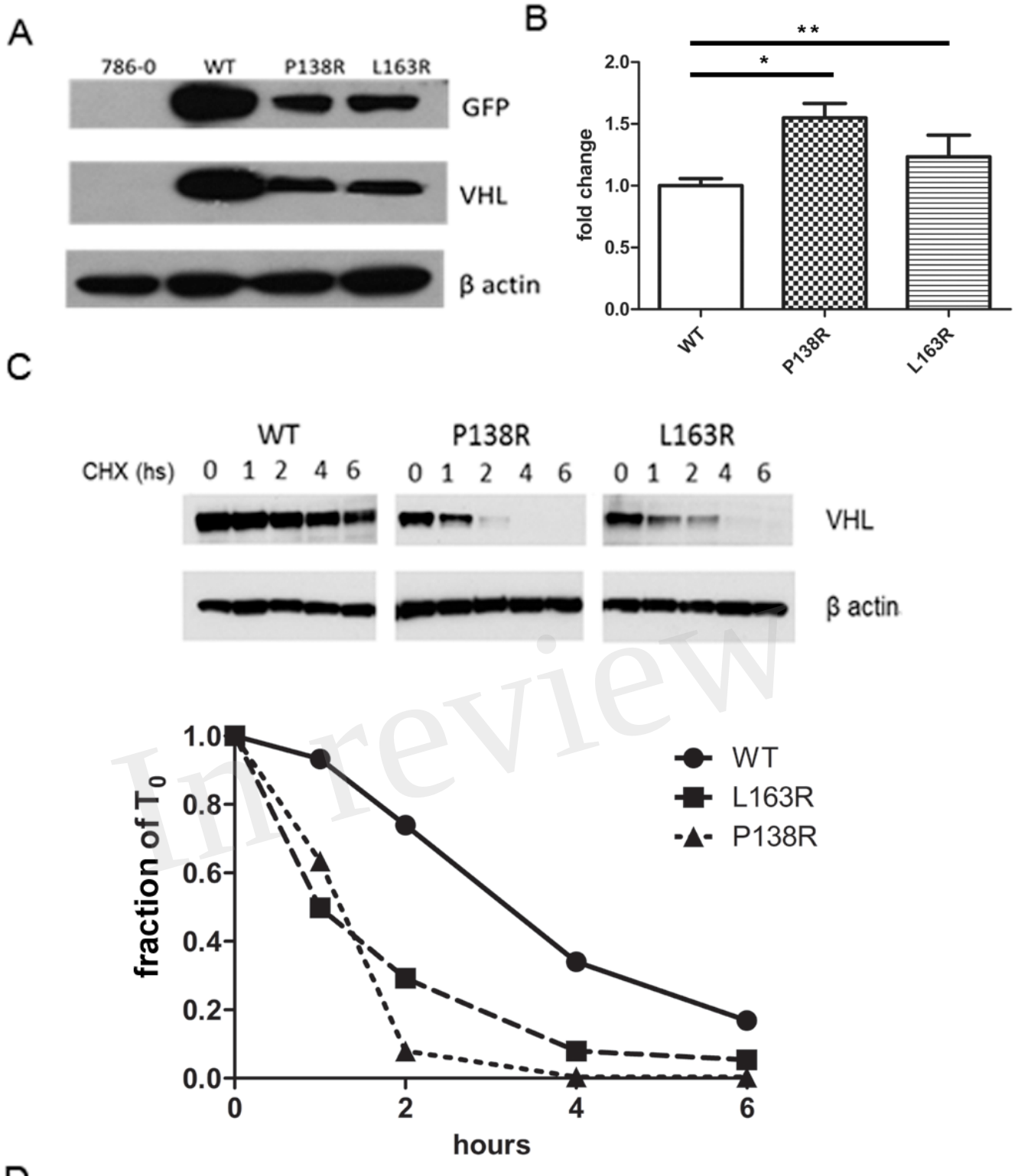

Figure 2.TIF

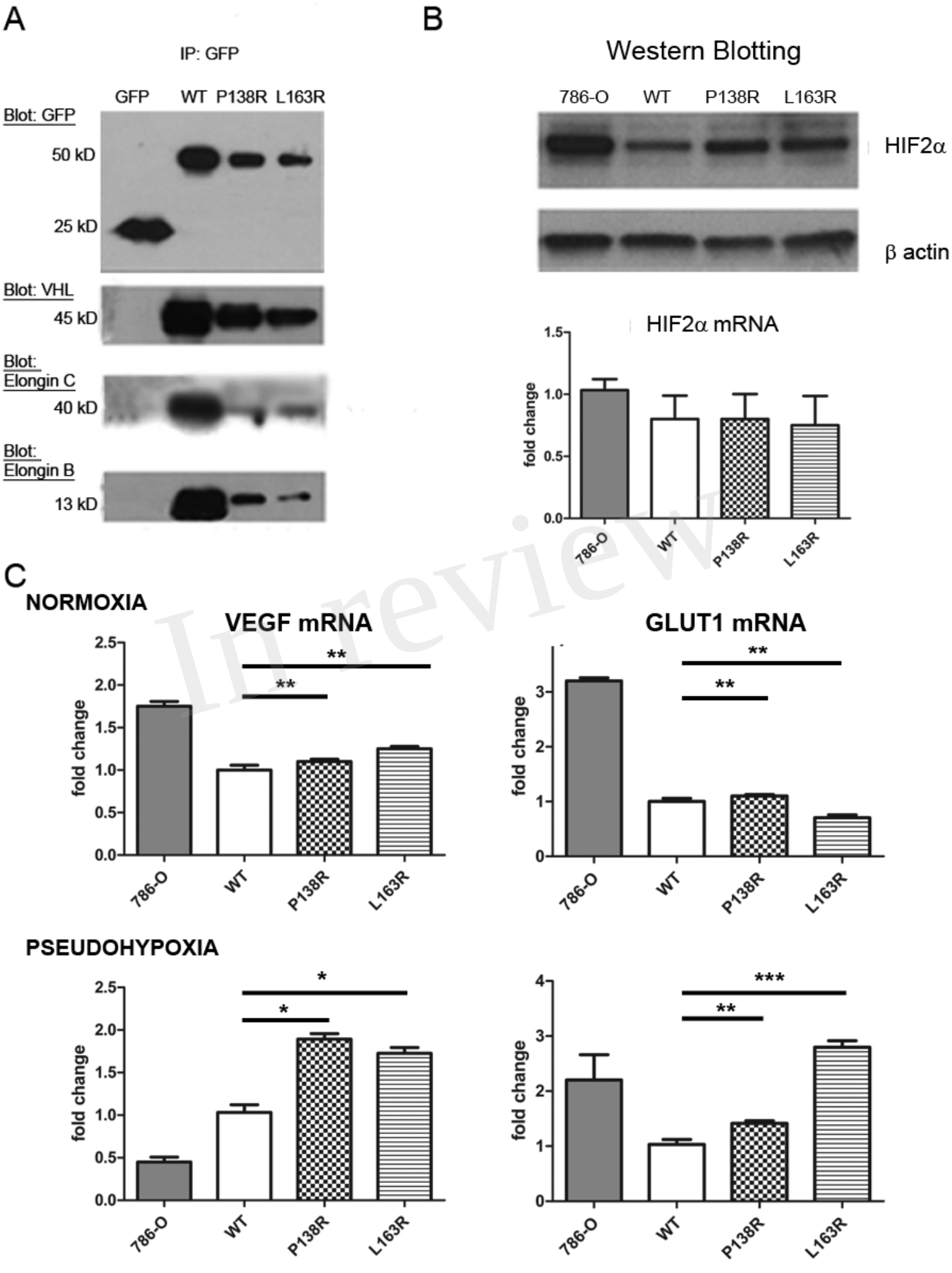

Figure 3.TIF

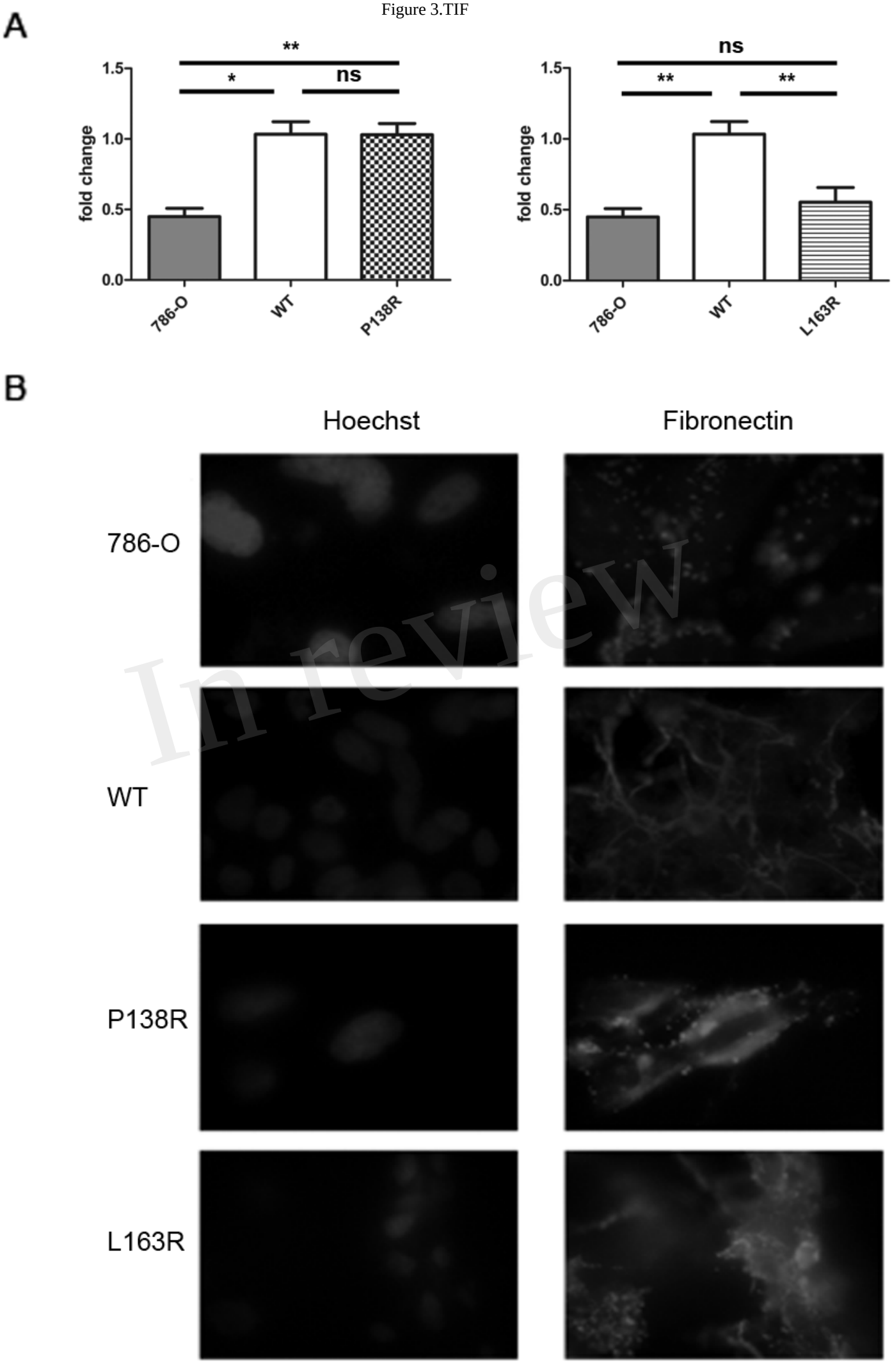

Figure 4.TIF

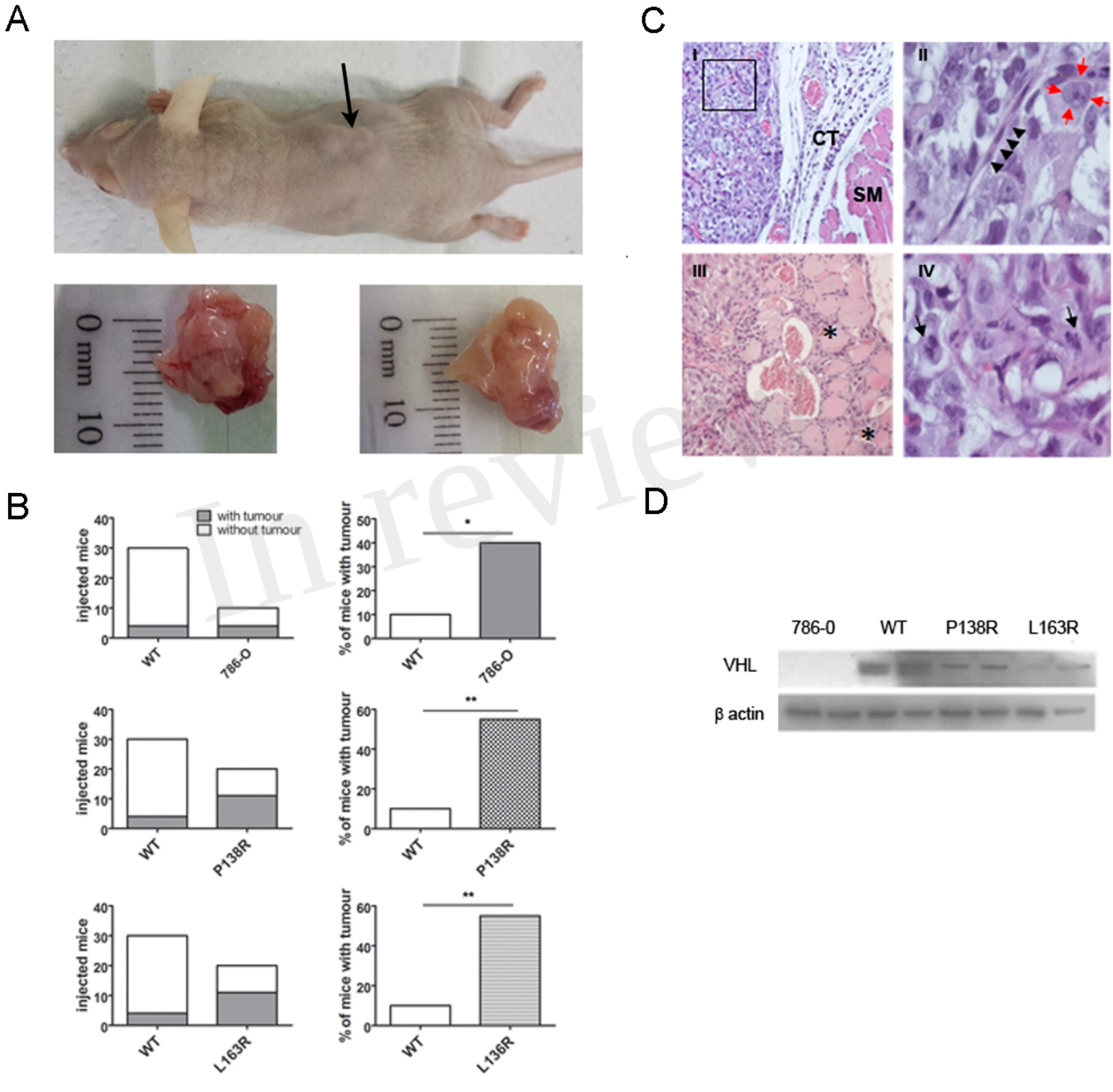
A
C
I
II
III
IV
CT
SM
B
with tumour
without tumour
injected mice
% of mice with tumour
WT
786-O
P138R
L163R
L136R
D
786-0
WT
P138R
L163R
VHL
β actin

Figure 5.TIF

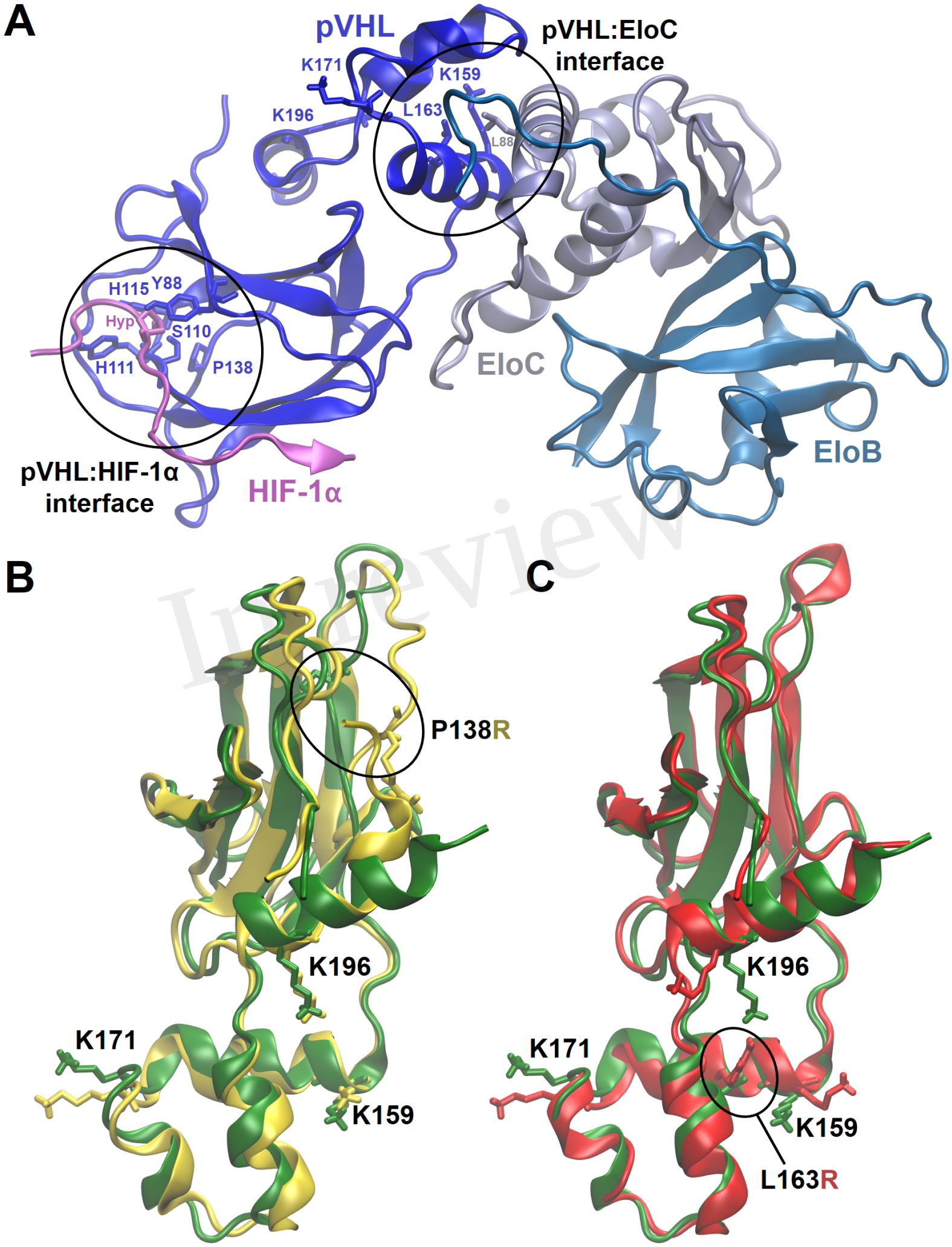

Figure 6.TIF

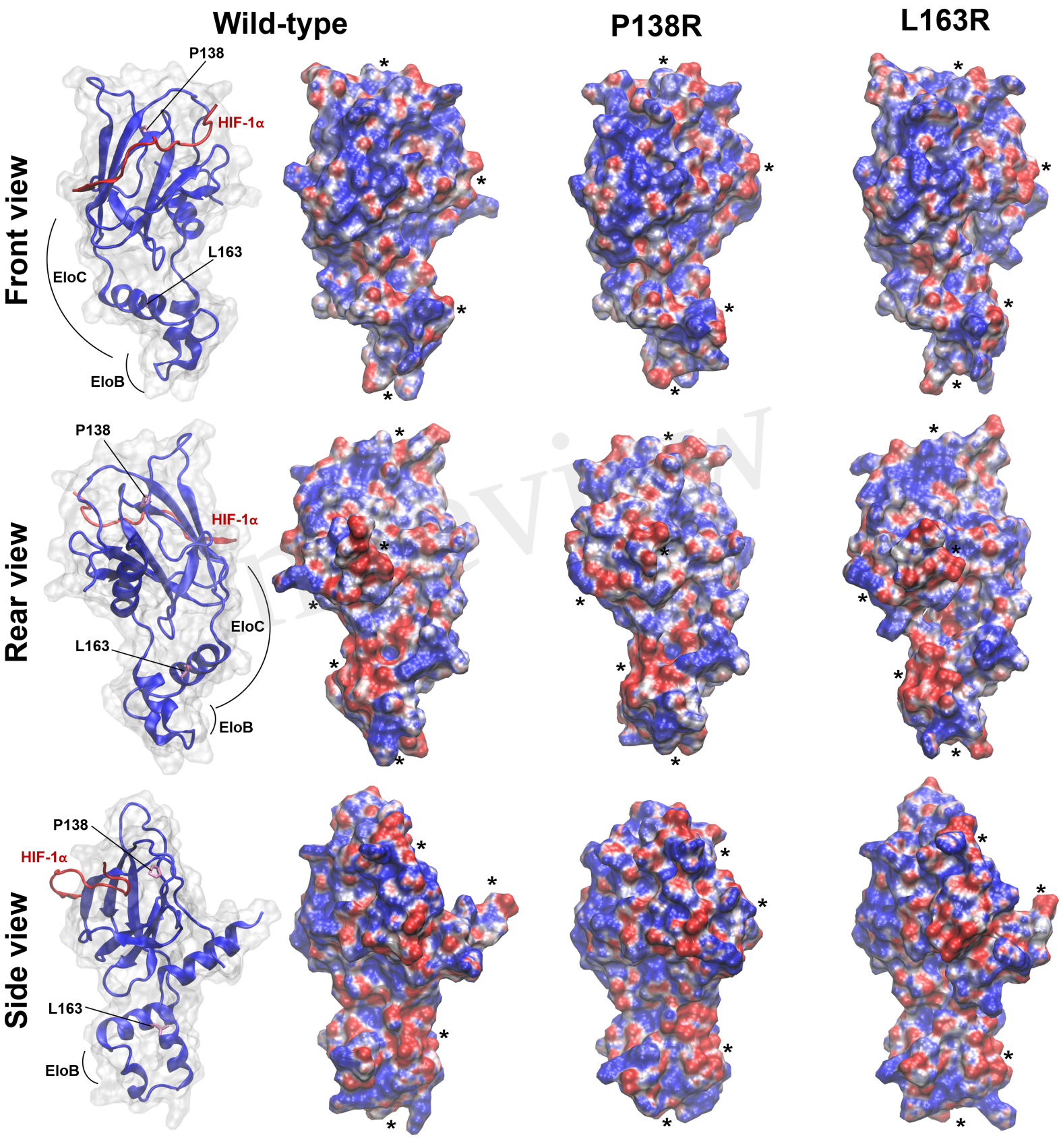
Wild-type
P138R
L163R
Front view
Rear view
Side view
P138
HIF-1α
L163
EloC
EloB